HHS Public Access

Author manuscript

Int J Radiat Oncol Biol Phys. Author manuscript; available in PMC 2024 July 31.

Published in final edited form as:

Int J Radiat Oncol Biol Phys. 2023 July 15; 116(4): 927–934. doi:10.1016/j.ijrobp.2023.01.007.

Preclinical evaluation of ^{89}Zr-Panitumumab for biology-guided radiotherapy

Arutselvan Natarajan[1,*], **Syamantak Khan**[2,*], **Xuanwei Liang**[3], **Hieu Nguyen**[2], **Neeladrisingha Das**[2], **David Anders**[1], **Noeen Malik**[1], **Oluwaseyi M. Oderinde**[4], **Frederick Chin**[1], **Eben Rosenthal**[5], **Guillem Pratx**[2]

[1]Department of Radiology, Stanford University, Stanford, CA

[2]Department of Radiation Oncology, Stanford University, Stanford, CA

[3]Department of Physics, Foothill College, Los Altos, CA

[4]RefleXion Medical, Hayward, CA

[5]Department of Otolaryngology, Vanderbilt University Medical Center, Nashville, TN

Abstract

Purpose: Biology-guided radiotherapy (BgRT) uses real-time line-of-response data from on-board PET detectors to guide beamlet delivery during therapeutic radiation. The current workflow requires ^{18}F-fluorodeoxyglucose (FDG) administration daily prior to each treatment fraction. However, there are advantages to reducing the number of tracer injections by using a PET tracer with a longer decay time. In this context, we investigated ^{89}Zr-Panitumumab (^{89}Zr-Pan), an antibody PET tracer with a half-life of 78 hours that can be imaged for up to 9 days using PET.

Methods and Materials: The BgRT workflow was evaluated pre-clinically in mouse colorectal cancer xenografts (HCT116) using small-animal PET/CT for imaging, and image-guided kilovoltage conformal irradiation for therapy. Mice (n=5 per group) received 7 MBq of ^{89}Zr-Pan as a single dose 2 weeks after tumor induction, with or without fractionated radiation therapy (RT; 6×6.6 Gy) to the tumor region. The mice were imaged longitudinally to assess the kinetics of the tracer over 9 days. PET images were then analyzed to determine the stability of the PET signal in irradiated tumors over time.

Results: Mice in the treatment group experienced complete tumor regression, whereas those in the control group were sacrificed due to tumor burden. PET imaging of ^{89}Zr-Pan showed well-delineated tumors with minimal background in both groups. On day 9 post-injection, tumor uptake of ^{89}Zr-Pan was 7.2 ± 1.7 in the control group vs 5.2 ± 0.5 in the treatment group (mean %ID/g ± SD; P = 0.07), both significantly higher than FDG uptake (1.1 ± 0.5 %ID/g) 1 hour post injection. To assess BgRT feasibility, the clinical eligibility criteria was computed using

Corresponding author: Guillem Pratx, PhD, pratx@stanford.edu.
*These authors contributed equally to this study.
Author responsible for statistical analyses:
Syamantak Khan, PhD

Conflict of interest statement:
GP reports finding from NIBIB and RefleXion Medical, inc.

human-equivalent uptake values that were extrapolated from preclinical PET data. Based on this semiquantitative analysis, BgRT may be feasible for 5 consecutive days following a single 740 MBq injection of ^{89}Zr-Pan.

Conclusions: This study indicates the potential of long-lived antibody-based PET tracers for guiding clinical BgRT.

Introduction

Biology-guided radiotherapy (BgRT) is a novel approach that integrates positron emission tomography (PET) into a linac-based radiotherapy (RT) system (1–6). The method uses a real-time PET signal to dynamically guide the delivery of the radiation treatment to static and even moving tumors. Leveraging the high sensitivity and specificity of PET data, BgRT potentially allows tighter margins than conventional treatments, reducing treatment toxicity. The RefleXion X1 is the first clinical system capable of delivering BgRT and is 510(k)-cleared in the United States for conventional radiotherapy (IMRT and SBRT) while awaiting clearance for PET-guided treatments (BgRT) (7–10). In addition to tumor motion management, BgRT is expected to have applications in the setting of oligometastatic disease, because the tumor-specific PET signal could enable the treatment of multiple PET-avid lesions in a single treatment session (11).

The current BgRT workflow uses ^{18}F-fluorodeoxyglucose (FDG) as the PET tracer to guide treatment delivery. FDG is a logical choice given its widespread use in the clinic and established reimbursement. However, because of its short half-life (110 min), a standard course of BgRT would require injections of the tracer for initial planning during the imaging-only simulation, and for each daily treatment fraction. In the standard protocol, FDG is administered intravenously by the clinical team, followed by a one-hour wait time for tracer uptake and clearance. Coordinating the injection of the tracer with the external beam treatment thus requires careful scheduling and coordination across departments. Repeated injections may also increase variability of the PET signal from day to day (12). In addition, they could contribute to patient discomfort, in part due to the requirement for fasting prior to each FDG session. In principle, reducing the number of PET injections could reduce cost and improve the clinical workflow of BgRT and the overall experience for patients.

In recent years, long-lived antibody-radiometal conjugates have been developed for PET imaging of various targets, including HER2, PDL1, CAIX and EGFR (13–15). These tracers use radioisotopes with long half-lives (i.e., 12 h or longer) that enable PET imaging for several days following injection to match the slow clearance of the antibodies from the blood pool. The purpose of this study is to assess whether a single injection of a long-lived PET tracer could guide BgRT over multiple days. Specifically, we investigated ^{89}Zr-panitumumab (^{89}Zr-Pan), a PET tracer targeting the epidermal growth factor receptor (EGFR), which is overexpressed in many tumors (16,17). This tracer has been investigated in 14 head-and-neck cancer patients at Stanford Medical Center (18). With its half-life of 78 hours, ^{89}Zr-Pan is capable of imaging EGFR-expressing tumors over several days (17).

In the proposed BgRT workflow, tracer administration would take place during simulation, obviating the need for additional injections on each treatment day.

However, a key challenge is whether the tumor will retain sufficient PET signal throughout the course of fractionated RT. Radiation-induced tumor cell death and shedding, altered EGFR expression, and radiolytic destruction of the PET probe could trigger a loss of ^{89}Zr signal from the tumor, hampering the ability of PET to successfully guide radiation delivery to the tumor in consecutive BgRT fractions. Therefore, a careful characterization of the PET signal within the irradiated tumor over multiple days is required. Toward this goal, we translated the BgRT workflow to the preclinical setting, using small-animal PET/CT for imaging and image-guided kV irradiation for therapy. Following a single injection of ^{89}Zr-Pan, we collected serial PET/CT images over 9 days in mice that received either no radiation or 40 Gy RT in 6 fractions (Figure 1). Finally, we analyzed the images to determine the feasibility of guiding BgRT using ^{89}Zr-Pan based on an established eligibility criterion.

Methods

Reagents, Antibodies, Radioisotopes and Cell Lines

All experimental reagents were obtained from Sigma-Aldrich (St. Louis, MO) unless otherwise stated. Panitumumab (20 mg/mL, Vectibix®; Amgen Inc, South San Francisco, CA), a fully humanized monoclonal antibody which inhibits the epidermal growth factor receptor (EGFR), was purchased from Stanford University Hospital Pharmacy (Stanford, CA). The radiometal chelator Desferrioxamine (Df-Bz-NCS (Df)) was obtained from Macrocyclics (Dallas, TX). ^{89}Zr was received from 3D Imaging (Little Rock, AR) with a specific activity of >111 GBq/μmol. High-performance liquid chromatography (HPLC) was performed on an HPLC-Ultimate 3000 (Thermo Scientific, Waltham, MA) with a size-exclusion chromatography (SEC) 2000 LC column (300 × 7.8 mm) using a 5 μm, hydrophilic-bonded silica support of 400-Å pore size (Phenomenex, Torrance, CA) with an ultraviolet detector and an online radioactivity detector. An instant thin-layer chromatography strip (Biodex Medical Systems, Shirley, NY) with saline as mobile phase was employed as an additional quality test for assessing the purity of the tracer.

The EGFR-expressing HCT116 cell line was purchased from the American Type Culture Collection (ATCC® number CCL-247, Manassas, VA) and maintained in McCoy's 5A medium, supplemented with 10% fetal bovine serum, 2 mmol/L glutamine, 100 units/mL penicillin, and 100 μg streptomycin. All media and additives were obtained from ThermoFisher Scientific (Waltham, MA).

Df-panitumumab synthesis, radiolabeling and quality control

Desferrioxamine (Df) was conjugated to panitumumab (5:1 ratio, 1 mg of Ab, 6.9 nmol) in 0.1 M $NaHCO_3$ buffer (pH=8.5 – 9.0) for 45 minutes. The precursor molecule of Df-panitumumab conjugate was purified from unconjugated Df molecules using size-exclusion chromatography (SEC-HPLC). Radiolabeling of Df-panitumumab was performed with ^{89}Zr (>111 GBq/μmol). ^{89}Zr was chelated to Df-panitumumab at a ratio of 192.4 MBq/mg of antibody in 0.5 M HEPES buffer (pH=7.0) at 37°C for 1 hour. The resulting ^{89}Zr-

panitumumab radioconjugate mixture was purified by radio-HPLC eluted at a flow rate of 1 mL/minute which was controlled by Chromeleon software (Sunnyvale, CA). The purified ^{89}Zr-panitumumab was determined by radioactive instant thin layer chromatography (radio-iTLC; AR-2000, Eckert & Ziegler, Valencia, CA) using a mobile phase of saline with 50 mM EDTA.

In vitro cell binding

The binding ability of the Df-panitumumab after conjugation was tested against unmodified panitumumab with HCT116 cells that were suspended in 1.5 mL microfuge tube (1×10^6 cells in 200 μL PBS). Panitumumab or Df-panitumumab (1 nM, 50 μL) was added to each tube (n=3) and the mixture was kept at 25°C. After 60 minutes, cells were pelleted by centrifugation (1000 ×g; 3 minutes), washed twice with PBS, and subsequently mixed with FITC-conjugated anti-human secondary antibody. After 30 minutes, cells were washed twice, and binding was measured using a FACSAria II sorter (BD Life Sciences, San Jose, CA). The binding affinity of the unmodified panitumumab and Df-panitumumab was compared to the signal obtained after staining with only the secondary antibody.

Animal studies

All animal experiments were conducted in compliance with the Guidelines for the Care and Use of Research Animals established by Stanford University's Administrative Panel on Laboratory Animal Care (APLAC). Female athymic nude *nu*/*nu* mice, 6 to 8 weeks of age, were obtained for these studies (Charles River Laboratories, Wilmington, MA). HCT116 cells (5×10^6) in Matrigel (Corning, Corning, NY) were injected (volume = 100 μL) into the left flank of the mice. The mice were assigned to the following groups: Group 1 (n=5) was imaged using ^{89}Zr-Pan and received RT. Group 2 (n=5) was imaged with ^{89}Zr-Pan but did not receive RT. Finally, Group 3 (n=4) was imaged with FDG and did not receive any treatment. Tumor volume was computed as $a^2b/2$, where a is measured using calipers along the short axis of the tumor, and b along the long axis. Euthanasia was performed by CO_2 inhalation followed by cervical dislocation.

Pre-clinical PET imaging

All mice were scanned using a GNEXT PET/CT scanner (SOFIE, Clover City, CA). PET radiotracer was administered as a single tail-vein injection 19 days after tumor induction, once all the tumors had reached >200 mm^3 in volume. This time point is referred to as "Day 0" thereafter. Mice from groups 1 and 2 received ^{89}Zr-Pan injections (6.9–7.4 MBq and 20–25 μg antibody per mouse) and were imaged on Days 1, 2, 3, 4, 6 and 9. We gradually increased the PET acquisition times from 10 initially to 20 minutes on Day 9 to compensate for the loss of signal caused by radioactive decay of the tracer. Mice from the third group received FDG injections (6.9 –7.4 MBq/mouse) on Day 0 and were scanned 1 h post-injection. Prior to scanning, mice were anesthetized with 2% isoflurane. Up to four mice were imaged simultaneously on the scanner.

Static PET images were co-registered with CT for organ identification using image analysis software (Inveon Research Workplace, Siemens). Tumor and thigh muscle regions of interest (ROIs) were contoured for every imaged mouse and every timepoint. Uptake by the tumors

was measured using IRW software with background and decay correction and expressed as percent of injected dose per gram of tissue (%ID/g). Tumor-to-muscle ratios were also computed. All longitudinal data were corrected for radioactive decay based on the 78-hour half-life of ^{89}Zr.

Image-Guided Conformal Radiation Therapy

Radiation treatment was given in 6 fractions of 6.6 Gy totaling 40 Gy, using an image-guided conformal irradiator (SmART, Precision X-ray Inc). Daily RT fractions were delivered a few hours after the corresponding PET imaging time point. Thus, in contrast to clinical BgRT, PET and RT were not performed simultaneously in this study. Each treated mouse was imaged daily using onboard cone-beam CT to ensure accurate coverage of the tumor by the radiation beam. Forward treatment planning was performed using RT_Image software (19). An example of treatment plan is shown in Figure S1. Treatment was delivered using two opposing beams collimated with 10 or 15 cm circular cones. Collimators with different diameters were chosen to appropriately match the size of the treated tumors. The beam parameters were 225 kVp, 13 mA, and 0.3 mm Cu filtration. Mice were anesthetized with 2% isoflurane during CT imaging and radiation treatment.

BgRT eligibility criteria

Once BgRT is implemented clinically, eligible patients will be selected for treatment based on the spatial distribution of the PET tracer in the tumor and surrounding normal organs. Patient eligibility is evaluated using two metrics: activity concentration (AC) and normalized tumor signal (NTS). For FDG, the AC and NTS thresholds are 5 kBq/cc and 2.7, respectively (20). However, for ^{89}Zr radiotracer, these thresholds have yet to be established and may likely change.

These empirical metrics are computed as follows. First, a biology-tracking zone (BTZ) is defined that encompasses the entire motion extent of the target tumor with additional margin to capture the localization error intrinsic to BgRT and patient set-up error. The AC metric is computed as the difference between the tracer concentration in the tumor and that in the background, where the former is assessed as the average uptake within the 80% BTZ isocontour line, and latter is computed as the average background within a 3 mm-thick shell around the BTZ. Importantly, the AC value represents the radioactivity physically present in the tumor at the time of the scan. Second, the NTS metric is assessed by dividing the AC value by the standard deviation of the PET image computed within the background region. In the current workflow, AC and NTS values are computed on PET images that are acquired on the X1 system during an imaging-only session. Patients who meet both criteria can then proceed to BgRT. The purpose of these criteria is to ensure that sufficient PET signal is available to guide the real-time delivery of the treatment, with no interference from surrounding FDG-avid organs. In the context of our study, PET images were acquired in murine subjects and thus the criteria could not be used directly to assess eligibility for BgRT. As a result, we extrapolated the mouse PET data to produce equivalent human-scale data, which we then used to compute the BgRT eligibility criteria (21). Briefly, tumor uptake was scaled linearly according to body weight and injected dose. These calculations assumed a weight of 25 g for mice, and for human, a weight of 75 kg and an injected tracer dose of 740

MBq. The overall passing rate was computed as the fraction of the treated mice that satisfied both AC and NTS conditions.

Statistical analysis

Statistical differences between two groups were calculated using unpaired, two-tailed Student's *t*-test. The level of significance is indicated as follows: *P < 0.05, **P < 0.01, ***P < 0.001. Statistical analyses were performed using Prism software (GraphPad, San Diego, California, USA) and Microsoft Excel.

Results

Radiolabeling and *in vitro* binding efficiency

The Df-radiometal chelate was conjugated to panitumumab at an initial ratio of 5 Df molecules per panitumumab mAb. After SEC-HPLC purification, the final immunoconjugate achieved a purity >99% and yielded 2–4 chelates/antibody, as determined by MALDI-MS (Figure S2). The radiolabeling of immunoconjugate yielded ~75% ^{89}Zr-panitumumab with a specific activity of 192.4 MBq/mg. The purity of the final ^{89}Zr-panitumumab was >98%, as evaluated both by radio-TLC and SEC-radio-HPLC (Table 1). The radiochemical properties of the synthesized PET tracer are summarized in Table 1.

Figure S3 shows *in vitro* binding affinity of panitumumab and Df-conjugated panitumumab (1 nM) to EGFR-expressing HCT116 cells (1×10^6 cells), as measured by flow cytometry. Mean fluorescence intensity (MFI) revealed that unmodified panitumumab and Df-conjugated panitumumab have similar affinity for HCT116 cells displayed (MFI ± SD: 448 ± 34 and 434 ± 25, respectively; n=3). Hence, Df conjugation did not substantially alter the target binding properties of the targeting antibody. These results indicate that the conjugated antibody is capable of targeting EGFR expression. In addition, EGFR expression in the HCT116 tumor xenograft model was confirmed by fluorescence immunohistochemistry (Figure S4). Tissue sections showed clear Alexa Fluor 594 signal, which confirms high EGFR expression of HCT116 tumor cells grown as xenografts.

Efficacy of radiation therapy

Tumor volume (mean mm^3 ± SD) measurements up to 60 days after tumor implantation show that the delivered dose of 6×6.6 Gy was sufficient to induce significant tumor regression in this mouse model (Figure 2). Compared to the untreated control group, the treated tumors started to visibly shrink starting 1 week after the beginning of the treatment, and continued to do so for over a month, to the point where their volume could no longer be accurately measured. The difference between the two groups reached the threshold for statistical significance (P<0.05) 3 weeks after treatment initiation. The mice continued to be monitored for another two months, with no visible evidence of local recurrence and no deaths directly attributable to the disease. In contrast, tumors in the control group reached the humane endpoint set in our protocol 40–49 days after tumor induction (Figure S5). Thus, we conclude that the chosen dose of 40 Gy was appropriate for testing the stability of ^{89}Zr-Pan after several fractions of BgRT.

Longitudinal PET/CT imaging of ^{89}Zr-Pan

To assess the stability of the PET signal, we compared the distribution of the tracer over time in both treated and untreated mice (Figure 3A). Images are shown along axial and coronal sections. The same intensity scale is used to facilitate comparison between treated and untreated mice. Clear uptake is visualized in the tumor region, confirming the ability of the tracer to target enhanced EGFR expression by HCT116 tumor cells *in vivo*. Over time, tumor contrast increased due to continued tumor uptake and simultaneous clearance of the tracer from the blood pool. By the end of the experiment (day 9), only minimal non-specific uptake could be seen in the liver and bones. Of note, a visual comparison of treated and untreated mice suggests a reduction in tracer uptake in the irradiated tumors compared to the corresponding controls. Finally, another set of n=4 untreated mice were imaged using FDG, currently the standard tracer for BgRT guidance. FDG uptake in this tumor model was relatively low compared to ^{89}Zr-Pan uptake, and the outline of the tumor could not be clearly visualized.

Quantification of *in vivo* PET signal in tumor ROIs confirmed our observations. Uptake of ^{89}Zr-Pan increased over time, both in terms of %ID/g (Figure 3B) and tumor-to-muscle ratio (Figure 3C). On Day 9, tumor uptake of ^{89}Zr-Pan was 7.2 ± 1.7 in the control group vs 5.2 ± 0.5 in the treatment group (mean %ID/g ± SD; P = 0.07), both significantly higher than FDG uptake (1.1 ± 0.5 %ID/g) 1 h post injection. Similarly, on Day 9, tumor-to-muscle ratio was 13.0 ± 5.5 in the control group and 7.1 ± 0.7 in the treatment group, which was also higher than the value measured for FDG (1.4 ± 0.3). Furthermore, tumor uptake (%ID/g) of ^{89}Zr-Pan reached a plateau on day 3, whereas tumor-to-muscle ratio continued to rise throughout the duration of the experiment, reflecting different contributions from tumor uptake and backround clearance to the overall contrast.

Additionally, ROI analysis demonstrates a notable decrease in uptake in irradiated tumors compared to untreated controls. By and large, the observed differences did not meet the threshold for statistical significance, except on Day 6 (P = 0.01) for the %ID/g uptake (Figure 3B) and on Day 2 for tumor-to-muscle ratios (P = 0.03; Figure 3C). The difference in uptake between the two groups was consistent over time and ranged from 3% to 40% (Figure 3B). Similar findings were also obtained for the tumor-to-muscle ratio, with differences ranging from 12% to 45% (Figure 3C). Thus, from these data, we conclude that, although exposure to RT caused a moderate decrease in tumor uptake, the tumors could still be visualized for up to 9 days, suggesting that the PET signal may still serve as a robust fiducial for BgRT guidance. Thus, to investigate the feasibility of BgRT using ^{89}Zr-Pan, we next considered the clinical criteria currently used to assess patient eligibility for this treatment.

BgRT eligibility criteria based on rescaled preclinical data

The eligibility of patients for BgRT is primarily determined by two empirical metrics, referred to as AC and NTS. These criteria were developed based on clinical studies in patients who were scanned on the RefleXion X1 system using FDG as the tracer. To apply the BgRT criteria to mouse data, we rescaled the measured tumor uptake values according to body weight and injected dose to yield human-equivalent data. The AC reflects radioactivity

available in the target tumor to guide BgRT delivery. The metric considers background signal in the region surrounding the tumor and must be greater than 5 kBq/cc for BgRT delivery. On Day 1 post injection, tumor uptake was too low to reach the AC criterion (Figure 4A). However, from Day 2 to Day 6, the criterion was met for at least 4 of the 5 mice. These mice also met the NTS criterion, which represents the strength of the signal with respect to system noise (Figure 4B). Hence, according to this methodology, BgRT may be feasible for up to 5 consecutive days following a single injection of ^{89}Zr-Pan (Figure 4C). In contrast, FDG uptake was too low in this tumor model to meet the AC requirements for BgRT.

Discussion

This study demonstrates the potential feasibility of BgRT using a single injection of ^{89}Zr-Pan, an antibody-based PET tracer with a half-life of 3 days. Data from our preclinical study demonstrates that a single injection of ^{89}Zr-Pan could provide image guidance for 5 consecutive fractions of BgRT. The significance of this finding is that ^{89}Zr-Pan could simplify the clinical workflow and obviate the need for multiple tracer administrations that lead to higher costs, patient discomfort, and day-to-day variability in tracer uptake.

A cornerstone of this strategy is the intrinsic trade-off between achieving sufficient radiation response and avoiding radiation-induced loss of PET signal. The selected dose regimen (40 Gy in 6 fractions) was sufficient to induce durable tumor control while avoiding unnecessary toxicity, with no detectable tumor relapse for up to 3 months post-treatment. Thus, the experiment challenged the stability of the ^{89}Zr tracking fiducial over an extended length of time in a scenario where tumor control is achieved.

By the end of the experiment, the PET signal in irradiated tumors was lower than that in unirradiated controls, either due to tumor cell death, loss of the EGFR target, or radiochemical degradation of the tracer. Yet, the loss of signal was only 30–45% and, in most cases, the difference was not statistically significant. Furthermore, it should be noted that tumor volume continued to increase for 9 days after treatment had started. This characteristic delay in the response of irradiated tumors creates a time window sufficient for ^{89}Zr-Pan retention at the tumor site, enabling efficient PET guidance before significant tumor shrinkage would occur. Furthermore, the moderate loss of tracer signal is compensated by the gradual background clearance of ^{89}Zr-Pan, resulting in an improved signal to background ratio. Taken together, these characteristics indicate that ^{89}Zr-Pan could be used clinically to guide BgRT, but the study will need to be repeated in humans given that RT could suppress the PET signal in the irradiated tumor.

While caution should be taken in extrapolating our finding to different tumor models and radiotherapy regimens, we speculate that the fundamental mechanism of EGFR-mediated ^{89}Zr-Pan uptake and retention will be the same in different settings, and we expect some degree of signal retention following irradiation in other models as well. For instance, tumors could be implanted orthotopically to emulate the clinically relevant scenario where non-specific uptake in normal organs could interfere with the performance of BgRT. Additionally, different tumor cell lines could be used to assess the impact of variable

EGFR expression and tumor radioresistance. Finally, different fractionation schemes could be investigated. Shorter fractionation scheme may accelerate the loss of PET signal but would also reduce the need for preserving PET signal at late timepoints. In contrast, longer fractionation schemes would require multiple injection due to the finite physical half-life the tracer.

Of note, our analysis suggests that 740 MBq of ^{89}Zr-Pan may be required to achieve tumor AC above the 5 kBq/cc threshold. This result was obtained by extrapolating human-equivalent tracer biodistribution from pre-clinical scans according to differences in body weight and injected dose. Other factors such as differences in metabolism, vascularization, EGFR target expression, and clearance kinetics were not considered in the extrapolation model, thus the rescaled biodistribution values should be taken as crude estimates and may only partially predict the behavior of the probe in humans. In addition, the sample size of 5 mice per group was relatively small, which contributes to increased uncertainty. In this context, the optimal dose of ^{89}Zr-Pan required for BgRT applications remains an open question. When used for diagnostic imaging, ^{89}Zr-Pan is administered as a single injection of ~30–60 MBq. The dose of 740 MBq proposed here will results in higher radiation exposure given the long half-life of the radionuclide and slow biological clearance of the labeled antibody. Potential toxicities of a treatment should be weighed against its likely benefits, as it is the case for other therapies such as radiopharmaceutical therapy. Another limitation of this study is that the ^{89}Zr-Pan data were evaluated using a criterion originally developed for FDG. Ideally, different thresholds for AC and NTS should be used for ^{89}Zr and ^{18}F to account for differences in positron yield and endpoint energy. Hence, the extrapolated biodistribution values should be taken as crude estimates that may only partially predict the radiotracer dose required for BgRT in humans.

A previous study in patients with head-and-neck squamous cell carcinomas (18) reported higher standardized uptake value (SUV_{max}) for ^{18}F-FDG than ^{89}Zr-Pan (11.6 vs. 3.4; $P < 0.001$), which is in contrast to our findings in murine HCT116 tumors. This discrepancy could be explained by a number of factors, including the high EGFR expression of HCT116 cells, the amount of injected radiotracer normalized to body weight, the kinetics of the tracer in mice and humans, and the early time point selected for imaging in the clinical study (74 ± 34 h post injection). Further investigation of these differences is needed.

Additionally, while antibodies can specifically target and label tumor cells, they have long circulation times, resulting in high background activity in the first 48 hours following injection. Accurate BgRT guidance requires the background signal to be minimal; therefore, ^{89}Zr-Pan would have to be administered 2 days prior to the first treatment fraction. As an alternative, smaller ^{89}Zr-labeled ligands, including peptides (22), affibodies (23) or antibody fragments (24), could be used to guide BgRT since these smaller molecules would be more rapidly cleared from the blood pool while still enabling imaging of specific tumor targets over an extended period of time. Faster clearance would also reduce the imaging dose for the patient. The long-term stability of small-molecule PET tracers under X-ray irradiation requires further investigation.

Conclusion

The current BgRT paradigm uses multiple injections of FDG to guide the delivery of each fraction. In contrast, long-lived antibody-based ^{89}Zr-Pan demonstrates tumor-specific uptake for up to 9 days after single-dose tracer administration, with only moderate loss of signal due to the radiotherapy treatment (<40%). This study suggests the potential of antibody-based PET for guiding clinical BgRT.

Supplementary Material

Refer to Web version on PubMed Central for supplementary material.

Acknowledgements:

The authors would like to dedicate this work to the memory of Dr. Sanjiv Sam Gambhir (1962–2020) for his mentoring and tremendous support through the years. Funding for this work was provided by RefleXion Medical, Inc. GP is supported by NIH grant 1R01EB03036701A1. We acknowledge core support for small-animal PET/CT imaging performed at the Stanford Center for Innovation in i*n Vivo* Imaging (SCi^3). The irradiator system was supported by NIH grant 1S10OD018208.

Funding statement:

This study was funded in part by RefleXion Medical, Inc.

Data sharing statement:

Research data will be shared upon request to the corresponding author.

References

1. Gaudreault M, Chang D, Hardcastle N, et al. Utility of biology-guided radiotherapy to de novo metastases diagnosed during staging of high-risk biopsy-proven prostate cancer. Frontiers in Oncology 2022;12.
2. Yang J, Yamamoto T, Mazin SR, et al. The potential of positron emission tomography for intratreatment dynamic lung tumor tracking: A phantom study. Med Phys 2014;41:021718. [PubMed: 24506609]
3. Fan Q, Nanduri A, Mazin S, et al. Emission guided radiation therapy for lung and prostate cancers: A feasibility study on a digital patient. Med Phys 2012;39:7140–7152. [PubMed: 23127105]
4. Fan Q, Nanduri A, Yang J, et al. Toward a planning scheme for emission guided radiation therapy (EGRT): FDG based tumor tracking in a metastatic breast cancer patient. Med Phys 2013;40:081708. [PubMed: 23927305]
5. Oderinde OM, Shirvani SM, Olcott PD, et al. The technical design and concept of a PET/CT linac for biology-guided radiotherapy. Clinical and Translational Radiation Oncology 2021;29:106–112. [PubMed: 34258399]
6. Hu Z, Bieniosek M, Ferri V, et al. Image-mode performance characterisation of a positron emission tomography subsystem designed for biology-guided radiotherapy (BgRT). Br J Radiol 2022;95:20220387.
7. Pham D, Simiele E, Breitkreutz D, et al. IMRT and SBRT treatment planning study for the first clinical biology-guided radiotherapy system. Technol Cancer Res Treat 2022;21:15330338221100231.
8. Shi M, Chuang CF, Kovalchuk N, et al. Small-field measurement and Monte Carlo model validation of a novel image-guided radiotherapy system. Med Phys 2021;48:7450–7460. [PubMed: 34628666]
9. Han B, Capaldi D, Kovalchuk N, et al. Beam commissioning of the first clinical biology-guided radiotherapy system. J Appl Clin Med Phys 2022:e13607. [PubMed: 35482018]

10. Simiele E, Capaldi D, Breitkreutz D, et al. Treatment planning system commissioning of the first clinical biology-guided radiotherapy machine. J Appl Clin Med Phys 2022:e13638. [PubMed: 35644039]
11. Shirvani SM, Huntzinger CJ, Melcher T, et al. Biology-guided radiotherapy: Redefining the role of radiotherapy in metastatic cancer. Br J Radiol 2021;94:20200873.
12. De Langen AJ, Vincent A, Velasquez LM, et al. Repeatability of 18F-FDG uptake measurements in tumors: A metaanalysis. J Nucl Med 2012;53:701–708. [PubMed: 22496583]
13. Okita R, Maeda A, Shimizu K, et al. PD-L1 overexpression is partially regulated by EGFR/HER2 signaling and associated with poor prognosis in patients with non-small-cell lung cancer. Cancer Immunol Immunother 2017;66:865–876. [PubMed: 28341875]
14. Parakh S, Lee ST, Gan HK, et al. Radiolabeled antibodies for cancer imaging and therapy. Cancers (Basel) 2022;14.
15. Stillebroer AB, Franssen GM, Mulders PF, et al. ImmunoPET imaging of renal cell carcinoma with (124)I- and (89)Zr-labeled anti-CAIX monoclonal antibody cG250 in mice. Cancer Biother Radiopharm 2013;28:510–5. [PubMed: 23697926]
16. Chang AJ, De Silva RA, Lapi SE. Development and characterization of 89Zr-labeled panitumumab for immuno–positron emission tomographic imaging of the epidermal growth factor receptor. Mol Imag 2013;12:17.
17. Lindenberg L, Adler S, Turkbey IB, et al. Dosimetry and first human experience with 89Zr-panitumumab. Am J Nucl Med Mol Imaging 2017;7:195. [PubMed: 28913158]
18. Lee Y-J, van den Berg NS, Duan H, et al. 89Zr-panitumumab combined with 18F-FDG-PET improves detection and staging of head and neck squamous cell carcinoma. Clin Cancer Res 2022.
19. Graves EE, Quon A, Loo BW Jr. Rt_image: An open-source tool for investigating PET in radiation oncology. Technol Cancer Res Treat 2007;6:111–121. [PubMed: 17375973]
20. Seyedin SN, Bassalow R, Mawlawi OR, et al. The potential of biology-guided radiation therapy in thoracic cancer: A preliminary treatment planning study. Front Oncol 2022;12.
21. Stabin MG. Steps in dose calculations Fundamentals of nuclear medicine dosimetry: Springer; 2008. pp. 76–118.
22. T DeJesus O Synthesis of [64Cu] Cu-NOTA-bn-GE11 for PET imaging of EGFR-rich tumors. Curr Radiopharm 2012;5:15–18. [PubMed: 21864245]
23. Garousi J, Andersson KG, Mitran B, et al. PET imaging of epidermal growth factor receptor expression in tumours using 89Zr-labelled ZEGFR: 2377 affibody molecules. Int J Oncol 2016;48:1325–1332. [PubMed: 26847636]
24. Fu R, Carroll L, Yahioglu G, et al. Antibody fragment and affibody immunopet imaging agents: Radiolabelling strategies and applications. ChemMedChem 2018;13:2466–2478. [PubMed: 30246488]

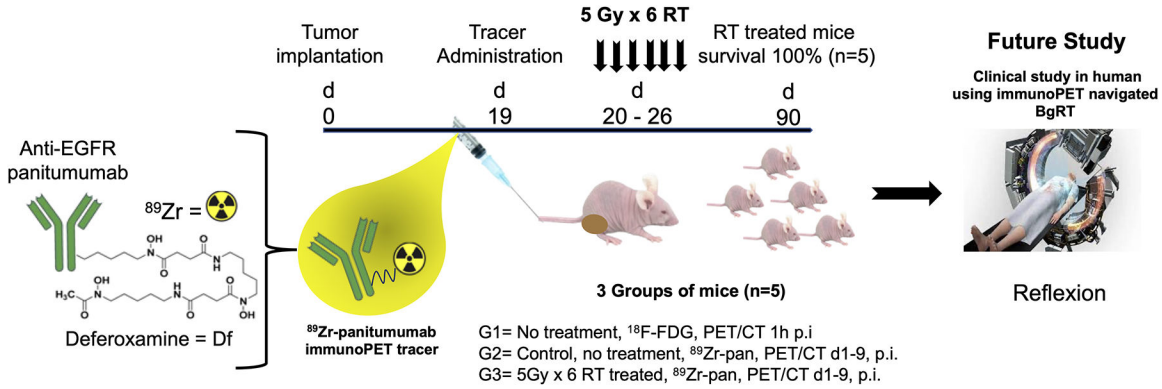

Figure 1.
Overall scheme of the study.

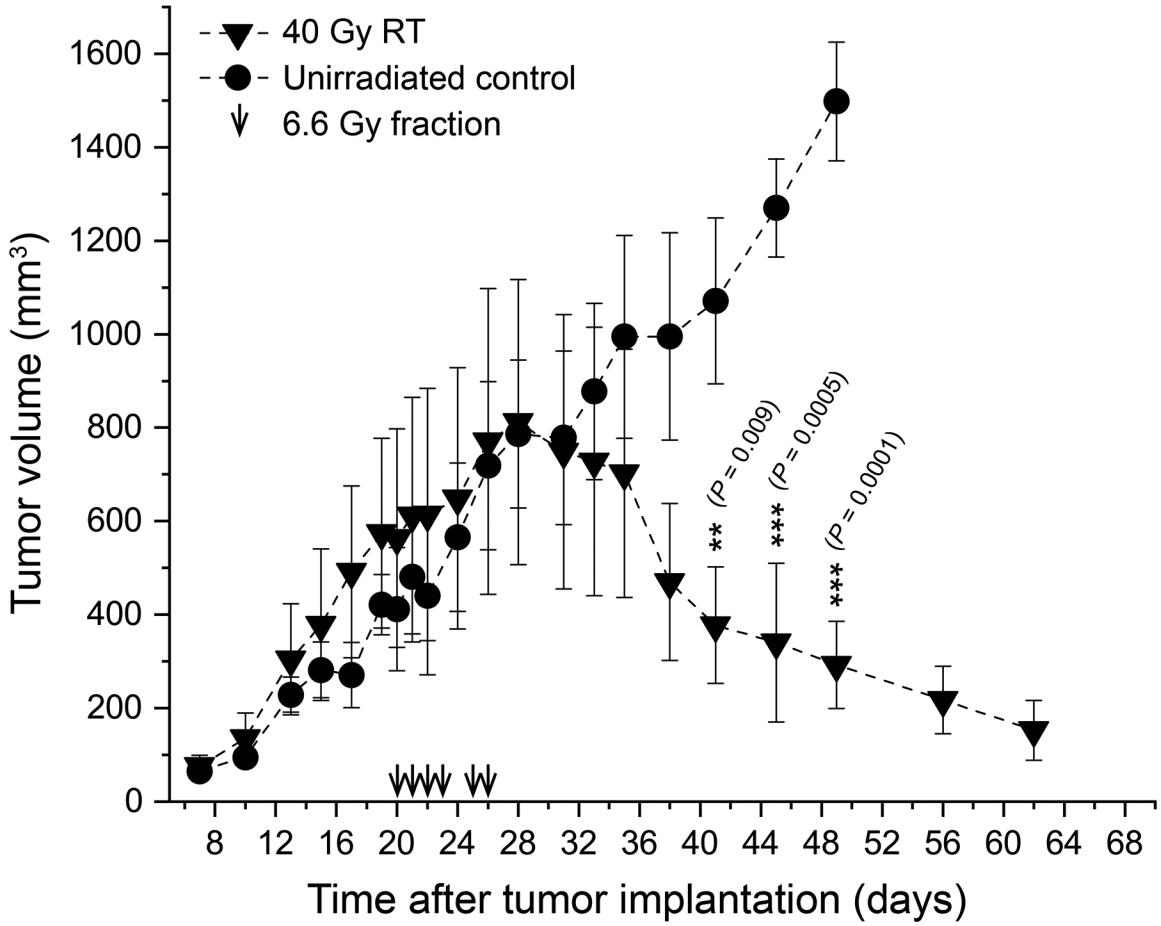

Figure 2.

Tumor growth kinetics. The investigated dose of 6×6.6 Gy enabled effective tumor control in the treated animals with no local recurrence, thus was clinically relevant to assess stability of PET signal under irradiation.

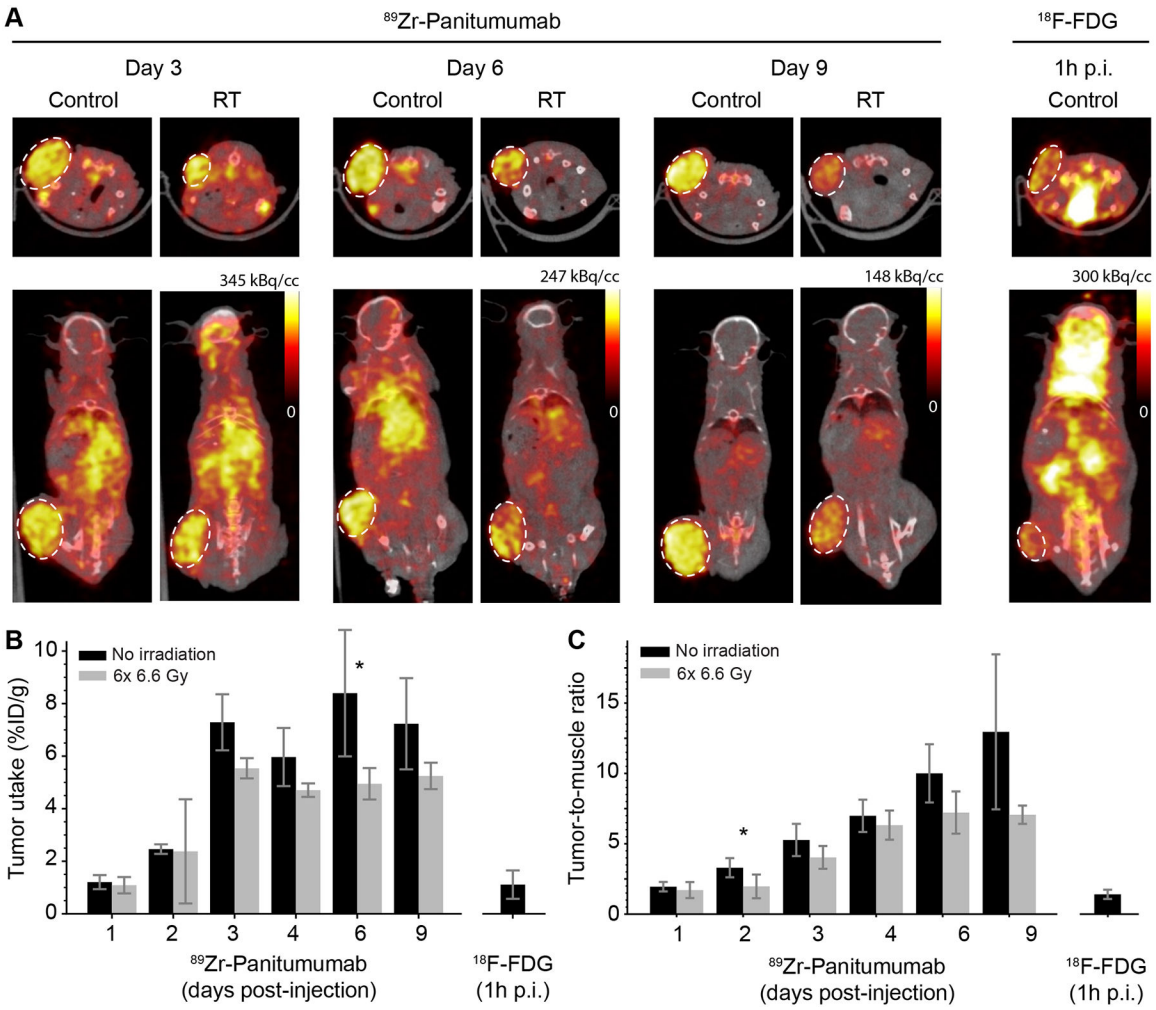

Figure 3.

PET imaging of ^{89}Zr-Pan. (**A**) Representative PET/CT images acquired on Day 3, 6 and 9 post-injection, showing untreated mice (control; n=5) and mice receiving 6×6.6 Gy radiation (RT; n=5). Representative FDG uptake is shown in the same tumor model (n=4), demonstrating lower contrast than ^{89}Zr-Pan. (**B**) Quantification of tumor uptake, expressed in terms of the percentage (%) of injected tracer dose per g of tissue, as a function of time. Although there is a consistent trend towards lower uptake in irradiated tumors, the difference between treated and untreated tumors meets the significance threshold only on Day 6 (* P = 0.01). (**C**) Quantification of tumor uptake, expressed as the ratio of tumor to muscle. Significance is only achieved on Day 2 (* P = 0.03). The differential uptake of ^{89}Zr-Pan in tumor vs muscle increases over time due to the specificity of antibody binding.

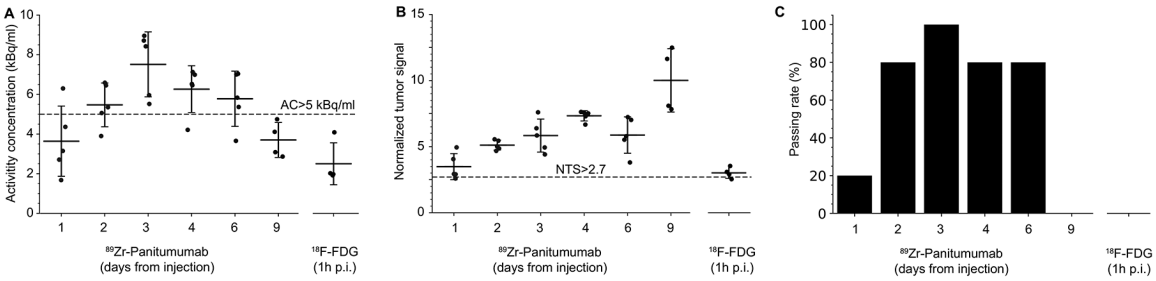

Figure 4.

Feasibility of BgRT based on clinical eligibility criteria. Mouse uptake data was rescaled according to body weight and injected dose to derive human-equivalent values. (**A**) The current X1 system requires the PET image to meet quantitative endpoints for BgRT to proceed. The activity concentration (AC) is the average tumor uptake within the 80% isocontour line, after background subtraction. The metric is shown for individual mice over time, with the 5 kB/cc threshold shows as a dashed line. (**B**) The normalized tumor signal (NTS) is the ratio of AC to the standard deviation within the background. The threshold for this metric is 2.7. (**C**) The passing rate represents the fraction of mice that met both AC and NTS criteria, and would theoretically be eligible for BgRT.

Table 1.

Characterization of Df-panitumumab (n = 3)

Characterization of ^{89}Zr-Df-panitumumab	
Purity of Df-panitumumab	>99%
Chelate to antibody ratio	2–4
Binding affinity of Df-pan relative to panitumumab	97%
Radiopharmaceutical purity by HPLC	>98%
Specific activity of ^{89}Zr-Df-panitumumab (MBq/mg)	192.4